Yu *et al*. *Dis Prev Res* 2024;3:11
**DOI:** 10.20517/dpr.2024.14

**Disaster Prevention and Resilience**

**Research Article**

**Open Access**

# The effect of FRP retrofitting on the seismic resilience of low-ductility RC frame structures: a case study

**Xiaohui Yu[1], Zenghui Li[1], Zhichao Jiang[2], Kuangyu Dai[3]**

[1]Guangxi Key Laboratory of Green Building Materials and Construction Industrialization, Guilin University of Technology, Guilin 541004, Guangxi Zhuang Autonomous Region, China.
[2]School of Civil Engineering, Harbin Institute of Technology, Harbin 150090, Heilongjiang, China.
[3]School of Civil Engineering, Zhengzhou University, Zhengzhou 450001, Henan, China.

**Correspondence to:** Dr. Kuangyu Dai, School of Civil Engineering, Zhengzhou University, No.100, Kexuedadao Road, Zhengzhou City, Zhengzhou 450001, Henan, China. E-mail: daikuangyu@zzu.edu.cn

**How to cite this article:** Yu X, Li Z, Jiang Z, Dai K. The effect of FRP retrofitting on the seismic resilience of low-ductility RC frame structures: a case study. *Dis Prev Res* 2024;3:11

**Received:** 5 Aug 2024 **First Decision:** 20 Sep 2024 **Revised:** 9 Oct 2024 **Accepted:** 20 Nov 2024 **Published:** 28 Nov 2024

**Academic Editor:** Jie Li **Copy Editor:** Fangling Lan **Production Editor:** Fangling Lan

## Abstract

This study investigates the effect of Fiber Reinforced Polymer (FRP) retrofitting on the seismic resilience of low-ductility reinforced concrete (RC) frame structures. The finite element model for low-ductility RC frame structures retrofitted with FRP wraps is established using OpenSEES. Fragility functions for low-ductility components before and after retrofitting are developed. Using the PACT software, the seismic resilience in terms of annual repair costs, repair time, casualties, and carbon emissions is evaluated for low-ductility RC frames w/wo FRP retrofitting. The results show that FRP retrofitting could improve the seismic resilience of low-ductility RC structures, especially at relatively low seismic intensities. Due to FRP retrofitting, the average annual repair cost, repair time, and carbon emission are reduced by 5.32%, 6.90%, and 7.16%, respectively. In addition, the FRP retrofitting would greatly improve human safety and almost no death would occur. Meanwhile, the annual average number of injuries is reduced by 57.6%.

**Keywords:** Seismic resilience, low-ductility reinforced concrete (RC) frame structures, FRP retrofitting, fragility function, seismic risk

## INTRODUCTION

Low-ductility reinforced concrete (RC) structures refer to those primarily designed to withstand vertical loads without specific seismic design considerations. Many such structures are constructed before 1976[1]. These structures are characterized by their limited capacity to deform and usually fail without significant strength degradation phenomena. They are particularly susceptible to seismic events because they easily cause brittle failure under earthquakes. Traditionally, low-ductility RC structures are designed without modern seismic considerations. This leads to inadequate reinforcement detailing that impairs energy dissipation and performance under dynamic loading[2].

Fiber Reinforced Polymer (FRP) has been widely applied in seismic retrofitting of concrete structures due to its advantages such as lightweight, high strength, corrosion resistance, and ease of construction. In recent years, numerous experimental and analytical studies have demonstrated the benefits of FRP retrofitting in improving the seismic capacity of RC structures. For example, Wang[3] examined the seismic performance of low-ductility frame structures reinforced by FRP using shake table tests. The results indicated that FRP retrofitting significantly reduced the maximum inter-story drift under identical seismic actions, and the retrofitted structure did not experience severe damage under the maximum considered earthquake (MCE). Yuksel *et al.* tested a one-story frame structure with infill walls and retrofitted with FRP by quasi-static tests[4,5]. The result showed the FRP-reinforced structures demonstrated significantly increased load-bearing capacity and reduced inter-story drift. Their study also revealed that FRP retrofitting could shift the structure from a collapse prevention limit state to a limited safety limit state based on performance-based seismic assessment. Kakaletsis[6] conducted quasi-static tests on a one-story planar frame to compare the carbon fiber-reinforced polymer (CFRP) retrofitting technique with other seismic retrofitting technologies. The results indicated that CFRP retrofitting effectively increased the load-bearing capacity and stiffness of the structure. However, CFRP-retrofitted structures were also prone to premature failure due to concrete and adhesive anchorage failure. Zhu *et al.* also investigated the seismic performance of RC frames before and after strengthening by FRP through experiments[7]. The results showed that CFRP-retrofitted frames exhibited excellent hysteretic energy dissipation capacity and high ductility, indicating superior seismic performance. Wang *et al.* tested scaled two-bay-two-story RC frame specimens strengthened using CFRP sheets[8]. The results demonstrated that the strengthening method involving wrapping CFRP can significantly improve the maximum horizontal bearing capacity, initial stiffness, and energy dissipation capacity of the low-ductility RC frame structure. Ghobarah and Said[9] conducted tests on externally strengthened beam-column joints in moment-resisting frames. The GFRP-strengthened joints showed a moderate improvement in failure load. Additionally, the tests revealed that the strengthened RC joint exhibited a slower rate of strength deterioration and a 60% higher ductility response. Dai *et al.* established a database of FRP-reinforced corroded RC columns[10]. The regression formulas of the nonlinear model parameters for FRP-reinforced corroded RC columns were developed. Abokwiek *et al.* tested 15 RC specimens with varying configurations under concentric and eccentric loading[11]. The results showed the strengthened specimens had significant increases in load-carrying capacity and ductility, with enhancements of up to 49% in axial loading and 95% in uniaxial bending. The above studies have demonstrated the superior performance of FRP materials in improving the seismic capacity of structures[12].

Recently, the assessment of seismic resilience of engineering structures has received significant attention from scholars worldwide. Several seismic resilience evaluation standards are introduced in various countries, such as FEMA P-58-1[13] and MCEER-09-2009[14] in the United States, and GB/T 38591-2020 in China[15]. Scholars have developed theoretical frameworks for assessing the seismic resilience of individual structures by incorporating seismic fragility theory and post-disaster loss assessment methods[16,17]. In structural seismic retrofitting engineering, incorporating resilience-based assessment methods allows for a comprehensive consideration of the performance of retrofitted structures and the consequences of post-earthquake losses[18]. This approach helps stakeholders to devise appropriate retrofitting strategies. However, resilience assessment methods have not been sufficiently addressed in the context of FRP seismic retrofitting projects, resulting in a lack

of understanding of the effect of FRP retrofitting on structural resilience.

Addressing this gap, this study focuses on the seismic resilience of low-ductility RC frame structures before and after FRP retrofitting. A low-ductility RC frame structure is designed and constructed, and finite element models of the structure before and after FRP retrofitting are established using OpenSEES. The fragility function of structural components also developed. Using the FEMA P-58 method, the seismic resilience indicators of the case structure are studied. By comparing multiple seismic performance indicators of the structure before and after retrofitting, the study identified the characteristics of resilience changes due to FRP retrofitting in low-ductility RC structures. The results of this study provide guidance for engineers in the seismic retrofitting of practical engineering projects.

## STRUCTURAL INFORMATION AND FINITE ELEMENT MODEL

### Structure information

A four-story RC frame structure has been designed. For the seismic hazard analysis presented later, the structure is assumed to be located in a site with a seismic fortification intensity of 7 degrees at 0.1g according to the existing codes[19,20] of China. The seismic design category is Group I, the site category is Class II, and the ground roughness is classified as C. The floor plan and elevation of the structure are shown in Figure 1. The structure is divided into ground floor and standard floors. The total construction area of the structure is 1,800 $m^2$. The height of the ground floor is 4.8 m, while the height of the standard floors is 4.2 m. The thickness of the floor and roof slabs is 120 mm. The design values for the dead load and live load of the roof are 6.9 and 2.0 $kN/m^2$, respectively. For the standard floors, the dead load and live load are 4.3 and 2.0 $kN/m^2$, respectively. For the corridors, the dead load and live load are 3.8 and 2.5 $kN/m^2$, respectively. The concrete strength used in the design is C30. Due to the low ductility structure usually only considers vertical loads during design, seismic fortification and wind loads are not considered in this structure. The cross-sectional dimensions and reinforcement details of the beams and columns in the structure are shown in Figure 2. The column cross-sectional dimensions are 400 mm × 400 mm, and the beam cross-sectional dimensions are 300 mm × 600 mm. The longitudinal reinforcement of beams and columns is HRB400. All other reinforcement uses HPB235. A finite element model is established for one span of the plane structure. The equivalent load distribution of the structure is illustrated in Figure 3.

### Finite element model

*Constitutive models of material*

(1) Reinforcement steel

The finite element model of the structure is established using the OpenSEES. The reinforcement steel is simulated using the Steel02 material model. This model represents the uniaxial constitutive behavior of the steel and includes isotropic hardening under cyclic loading. This allows it to accurately capture the stress-strain relationship of the steel under repeated loading. The stress-strain constitutive relationship is expressed as:

$$\sigma^* = b\varepsilon^* + \frac{(1-b)\varepsilon^*}{(1+\varepsilon^{*R})^{1/R}} \tag{1}$$

where $\sigma^*$ and $\varepsilon^*$ are the normalized stress and strain, respectively; their calculation expressions are given by

$$\sigma^* = \frac{\sigma - \sigma_r}{\sigma_0 - \sigma_r} \tag{2}$$

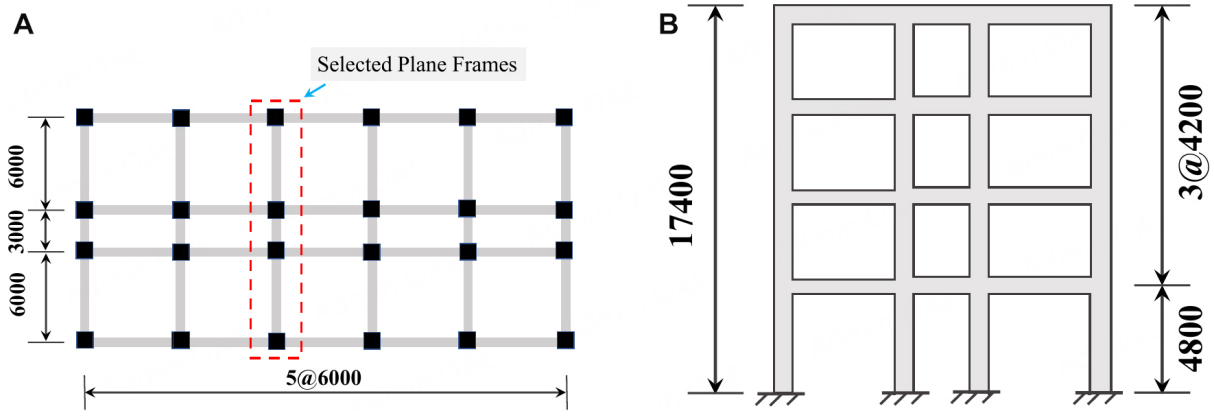


**Figure 1.** Plan and elevation view of structure. (A) Plan view; (B) Elevation view.

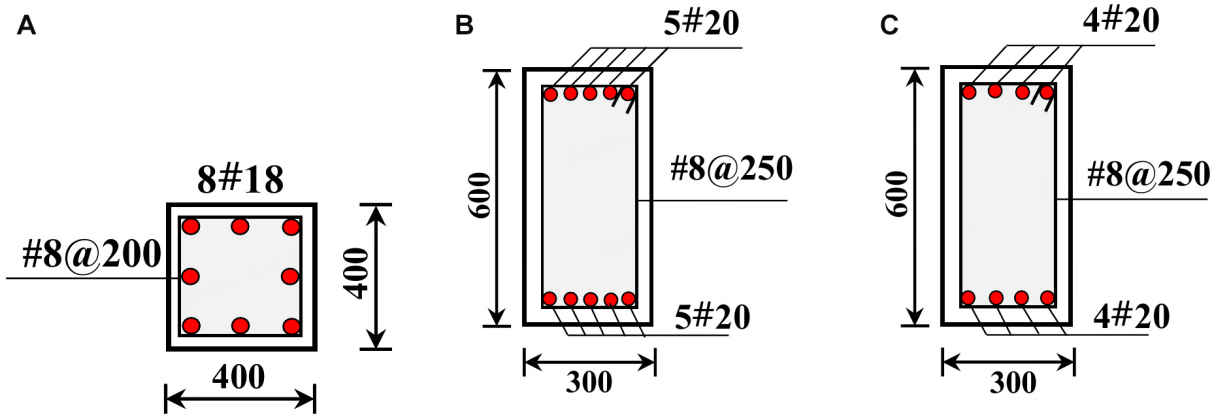


**Figure 2.** Structural reinforcement information. (A) Column; (B) Beam of standard floor; (C) Beam of roof.

$$\varepsilon^* = \frac{\varepsilon - \varepsilon_r}{\varepsilon_0 - \varepsilon_r} \tag{3}$$

where $R$ is a parameter that influences the shape of the transition curve, and its calculation expression is given by

$$R = R_0 - \frac{a_1 \xi}{a_2 + \xi} \tag{4}$$

where $b$ is the strain hardening ratio, which is set to 0.00085 in this study. The values of $R_0$, $a_1$ and $a_2$ are taken as 18, 0.925, and 0.15 according to the recommendations in OpenSEES, respectively.

(2) Concrete

The unconfined concrete regions and the regions confined only by stirrups are simulated using the Concrete01 material model. The peak stress-strain relationship is based on the constitutive model proposed by Scott *et al.*[21]. The confining effect of the stirrups on the concrete is accounted for through a confinement factor. The stress-strain expressions are given by:

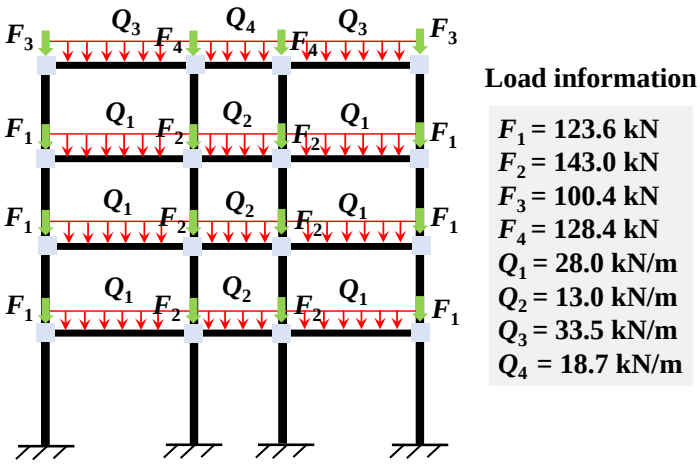


**Figure 3.** Equivalent load distribution of the structure.

$$\sigma_c = f_{pc}\left[\frac{2\varepsilon_c}{\varepsilon_{pc}} - \left(\frac{\varepsilon_c}{\varepsilon_{pc}}\right)^2\right], \text{for } 0 \le \varepsilon_c \le \varepsilon_{pc} \tag{5}$$

$$\sigma_c = \frac{f_{pc} - f_{cu}}{\varepsilon_{pc} - \varepsilon_{cu}}(\varepsilon_c - \varepsilon_{cu}), \text{for } \varepsilon_{pc} \le \varepsilon_c \le \varepsilon_{cu} \tag{6}$$

$$\sigma_c = f_{cu}, \text{for } \varepsilon_c \ge \varepsilon_{cu} \tag{7}$$

where $\sigma_c$ and $\varepsilon_c$ represent the compressive stress and the corresponding compressive strain of the concrete, respectively; $f_{pc}$ and $\varepsilon_{pc}$ are the compressive stress and corresponding strain at the peak point, respectively; $f_{cu}$ and $\varepsilon_{cu}$ are the compressive stress and corresponding strain at the ultimate point, respectively.

(3) Stress-strain constitutive model for FRP-reinforced concrete

The model proposed in reference [3] is used to account for the confinement effect of FRP on RC square columns. FRP-confined concrete components typically exhibit three failure modes: strong, moderate, and weak confinement modes. In the strong confinement mode, the failure of a column is characterized by the crushing of the concrete, immediately followed by the rupture of the FRP material. In the moderate confinement mode, the concrete is crushed first, and then the FRP material ruptures after undergoing some deformation. The weak confinement mode occurs when the FRP material fails prematurely due to either an insufficient number of FRP wrapping layers or adhesive anchorage failure. According to the research in reference [3], when the adhesive is intact and the number of FRP reinforcement layers exceeds two, the weak failure mode is unlikely to occur in FRP-confined concrete components. Since the retrofitting scheme discussed later involves at least two layers of FRP, this paper assumes that all components exhibit strong confinement failure modes. The stress-strain relationship of concrete before and after FRP confinement is given in Figure 4.

The ultimate stress and strain for concrete confined by FRP are defined as follows:

$$\frac{f_{cu}}{f_c'} = 0.2 + 0.59\left(\frac{f_{1s}}{f_c'}\right)^{0.20} + 3.47\left(\frac{f_{1f}}{f_c'}\right)^{0.64} \tag{8}$$

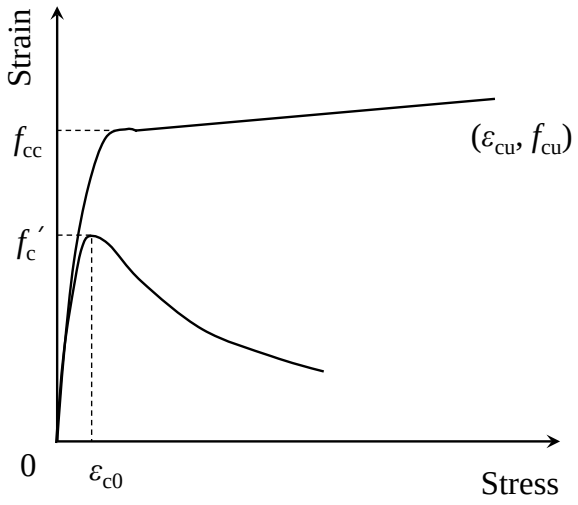


**Figure 4.** Stress and strain relationship of concrete before and after FRP confinement.

$$\frac{\varepsilon_{cu}}{\varepsilon_{c0}} = 2 + 5.06\left(\frac{f_{1s}}{f_c'}\right)^{0.03} + 73.31\left(\frac{f_{1f}}{f_c'}\right)^{1.07} \tag{9}$$

where $f_c'$ and $\varepsilon_{c0}$ are the peak stress and peak strain of unconfined concrete, respectively; $f_{cu}$ and $\varepsilon_{cu}$ are the ultimate compressive stress and the peak compressive strain of FRP-confined concrete, respectively; $f_{ls}$ and $f_{lf}$ are the effective lateral confining forces provided by stirrups and FRP, respectively.

The peak stress and strain of FRP-confined RC square columns are given by:

$$f_{cc} = f_c'\left(1 + 0.35\lambda_f + 0.50\lambda_h + 0.85\lambda_1\right) \tag{10}$$

$$\varepsilon_{cc} = \varepsilon_{c0}\left(1 + 2.0\lambda_f + 2.5\lambda_h\right) \tag{11}$$

$$\lambda_f = \frac{\kappa_a \rho_f f_f}{f_c'} \tag{12}$$

$$\lambda_h = \frac{\rho_{st} f_{yt}}{f_c'} \tag{13}$$

$$\lambda_1 = \frac{\rho_g f_f}{f_c'} \tag{14}$$

where $f_{cc}$ and $\varepsilon_{cc}$ are the peak compressive stress and strain of FRP-confined concrete, respectively; $\kappa_a$ is the shape factor, defined as the ratio of the effective confined area to the total cross-sectional area; $\lambda_f$ is the characteristic value of the FRP confinement; $\lambda_h$ is the characteristic value of the stirrup confinement; $\lambda_l$ is the

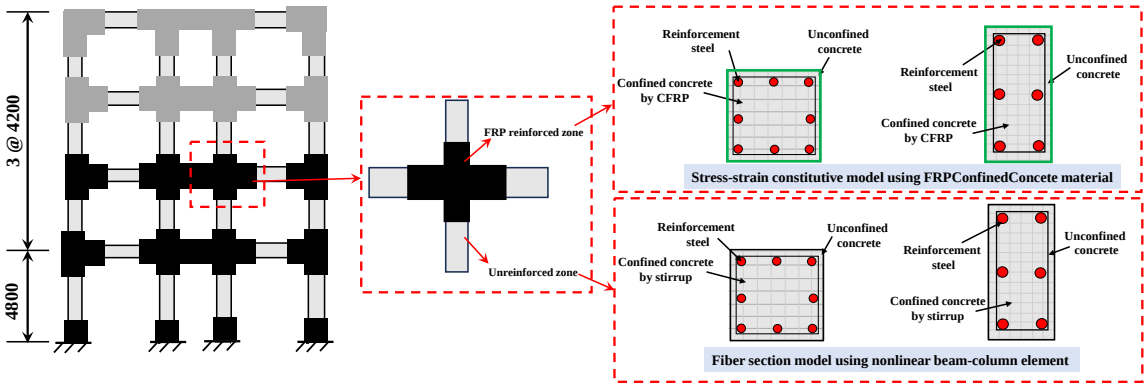


**Figure 5.** Finite element model.

characteristic value of the longitudinal reinforcement; $\rho_g$ is the longitudinal reinforcement ratio, excluding the radius of the chamfer; $\rho_{st}$ is the volumetric stirrup reinforcement ratio; $\rho_f$ is the volumetric reinforcement ratio provided by transverse FRP; $f_f$ is the ultimate strength of the FRP, and $f_{yt}$ is the yield strength of the stirrups.

*Sections and elements*

The finite element of structure is established using the distributed plasticity nonlinear beam-column elements in OpenSEES, as shown in Figure 5. For unreinforced beams and columns, only one element is needed. They are simulated using a fiber section element. For FRP-reinforced RC beams and columns, each component is simulated with three displacement-based nonlinear beam-column elements. These elements represent three regions, including the two ends, which are the plastic hinge reinforced zones and the middle unreinforced zone. Each of these regions is simulated with one nonlinear beam-column element considering distributed plasticity. The number of integration points along the element is 10. Zero-length section elements are used at the roots of beams and columns, and Bond-SP01 material is adopted to consider bond-slip between reinforcement steel and concrete. The element for the unreinforced middle zone is modeled using a fiber section. The number of fibers over a geometric cross-section is 400. The elements for the reinforced zones use the stress-strain constitutive model of FRP-RC. Therefore, the OpenSEES material named FRPConfinedConcrete[3] material is used. The hysteresis rule of FRPConfinedConcrete material in this paper could accurately reflect the stress-strain relationship and the deterioration of concrete under cyclic compression. It is determined based on cyclic compression tests of FRP-confined concrete columns. This is a significant improvement when compared to Concrete01 material models, which only modified the backbone curve for monotonic compression, while the hysteresis rule is developed by the test of normal concrete. For a detailed comparison, see the literature[3]. It should be noted that the unloading curve is simplified using a two-segment approximation, while the rest of the envelope curve, residual strain, and other aspects are consistent with the relationship described in Section "Constitutive models of material". During the dynamic analysis, the base of the structure is considered rigid, and the convergence tolerance is set to $1.0 \times 10^{-8}$. In addition, since this paper is concerned with the seismic performance of the structure as a whole, local geometric imperfection is not considered.

*Model validation*

The modeling method described above is validated using specimens S1H2C0N2 and S1H1C4N2 from reference[22]. Both specimens are column components with an axial compression ratio (ACR) of 0.45. The S1H2C0N2 specimen is a low-ductility specimen, while the S1H1C4N2 has the same design details as the S1H2C0N2. The difference is S1H1C4N2 specimen is reinforced with four layers of CFRP compared to S1H2C0N2. Figure 6 compares the experimental result with the predicted result, showing that the simulation method employed in this study effectively captures the degradation characteristics of low-ductility columns

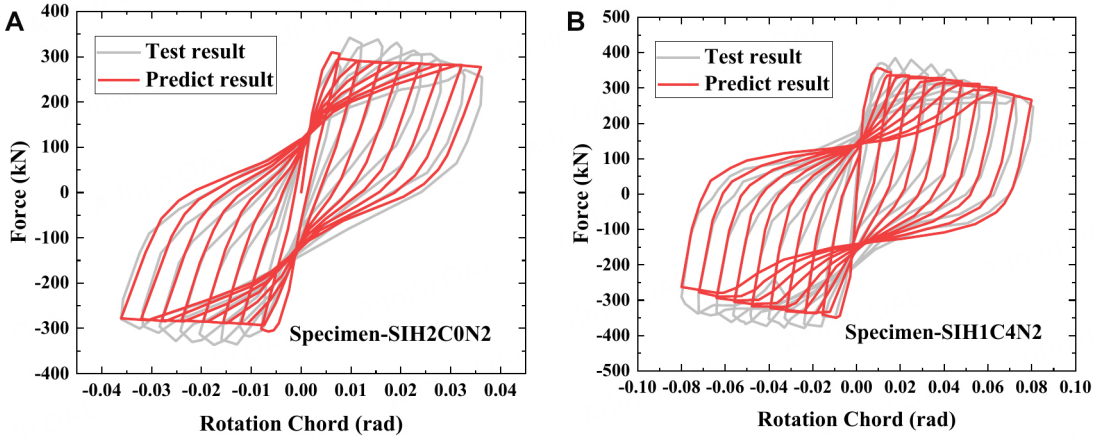


**Figure 6.** Test and predict result for low-ductility column and FRP reinforced low-ductility column. (A) Low-ductility column; (B) Low-ductility column reinforced with CFRP.

and the seismic performance improvements brought by FRP retrofitting.

### Retrofitting scheme

The Pushover analysis of the low-ductility structure model shows that the maximum inter-story displacement occurs in the lower-middle floors, with a noticeable stiffness discontinuity in the middle floors. Therefore, the bottom two floors are identified as the weak stories under seismic loads. According to existing standards [23,24], the components in weak stories are reinforced with four layers of FRP confinement. For the non-weak story components, two layers of FRP confinement are applied to prevent the stiffness of the bottom two floors from becoming excessively strong compared to the upper floors after FRP retrofitting [23]. Considering the moment above, the following FRP retrofitting schemes are proposed, as illustrated in Figure 7. In Figure 7, the bottom two floors (1-2 floors) have columns reinforced at their ends by wrapping FRP. The retrofitting height is 1.5 times the column cross-section height. The beam ends are wrapped with four layers of FRP laterally and two layers of FRP longitudinally, with a retrofitting length of two times the column cross-section height. The middle span of the beams is full-length reinforced. The top two floors (3-4 floors) are reinforced in the same positions as the 1 and 2 floors but with half the number of FRP layers. This study assumes the use of a unidirectional CFRP fabric with a weight of 300 g/m$^2$ for retrofitting the structure. Each layer has a thickness of 0.167 mm, an elastic modulus of 244 GPa, an ultimate tensile strength of 4,340 MPa, and an ultimate tensile strain of 0.018. For ease of description later, the unreinforced low-ductility structure is named Case-1, while the FRP-reinforced low-ductility structure is named Case-2.

## SEISMIC RESILIENCE ANALYSIS MODELS

### Assessment framework

The FEMA P-58 methodology, combined with the PACT software, is used to conduct a time-based performance assessment of low-ductility structure (Case-1) and FRP-reinforced low-ductility structure (Case-2). This assessment method evaluates the seismic performance indicators of the building structure under all possible seismic intensities over a specified period (50 years in this study) to determine the annual exceedance frequency and the annual average value of the building performance indicators during its service life.

### Building replacement model

*Replacement cost model*

Assume the structure is located in Weihai, China, and its intended use is as an office building. The construction cost of the structure is set as the replacement cost. According to the China Construction Engineering Network

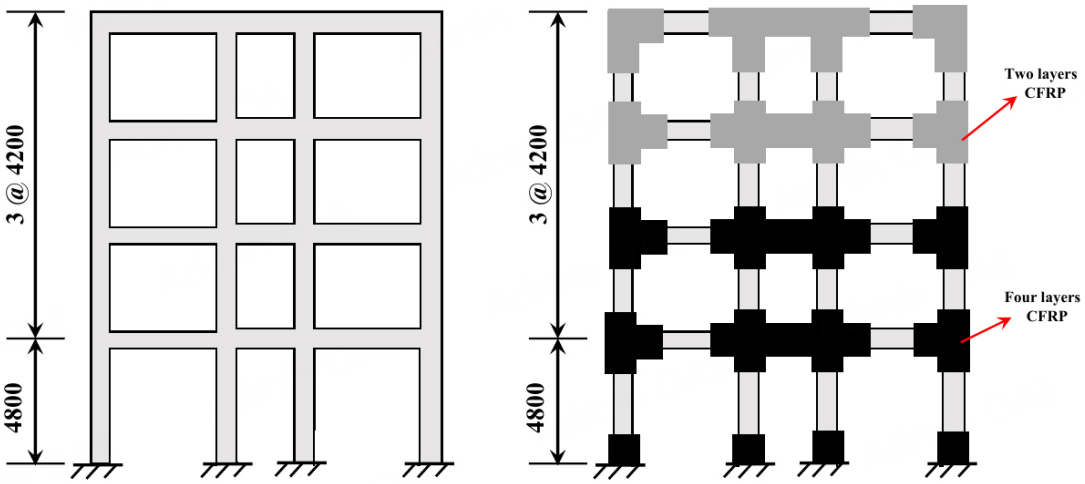


**Figure 7.** Retrofitting scheme. (A) Case-1; (B) Case-2.

(CCEN)[25], the replacement cost for Case-1 is calculated to be $558,000. For Case-2, the FRP retrofitting cost is determined by combining the seismic retrofitting pricing norms of Sichuan Province[26] and current prices for FRP materials and labor in China. The retrofitting cost is about $135,000. This retrofitting cost is added to the replacement cost of Case-1 to obtain the total cost for Case-2. As noted in FEMA P-58[13], many property owners prefer to replace structures when the estimated repair costs surpass approximately 40% to 50% of the replacement cost[27]. Therefore, a repair limit coefficient of 0.5 is set. When repair costs reach the repair cost limit, no further repairs will be made to the structure, and the repair costs will be considered replacement costs.

*Replacement time model*

The building replacement time is estimated based on the method proposed by Zhu[28], assuming the structure is a typical civilian building. The construction period for the part of the building below zero elevation can be set to 25 days when the land is labeled as Class II, with no basement and a ground floor area of less than 500 $m^2$. For the part above zero elevation, according to the stories (4 stories), occupy (office building), and the area (less than 3,000 $m^2$), the construction period for the above-ground part is calculated to be 230 days. After considering a standard 7-day period for building demolition, the total replacement time for this four-story building is 262 days.

*Carbon emissions model*

According to GB/T 51366-2019[29], the carbon emissions from building replacement are equivalent to the carbon emissions during the production stage. This includes the total carbon emissions from the production and transportation processes of building materials (concrete, steel, CFRP fabric). The calculation methods are given in

$$E^{pro} = E^{mat} + E^{tra} \tag{15}$$

$$E^{mat} = \sum_i Q_i^{mat} EF_i^m \tag{16}$$

$$E^{tra} = 10^{-3} \sum_{k} \sum_{i} Q_{ik}^{tra} EF_{k}^{t} \tag{17}$$

where $E^{mat}$ is the carbon emissions from the production process of materials; $E^{tra}$ is the carbon emissions from the transportation process of materials; $Q_i^{mat}$ is the consumption quantity of material $i$; $EF_i^m$ is the carbon emission factor for material $i$; $Q_{ik}^{tra}$ is the freight volume of material $i$ transported by mode $k$; $EF_k^t$ is the carbon emission factor per unit freight volume for transportation mode $k$.

Assume the transportation distances from production to use are 40 km for concrete, 500 km for steel, and 500 km for CFRP fabric. The calculated carbon emissions are presented in Table 1, with the total carbon emissions for Case-1 and Case-2 being 2111.56 $tCO_{2e}$ and 2183.91 $tCO_{2e}$, respectively.

### Structural occupancy and population density model

According to GB 50189-2015 [30], a model is developed in this study to reflect the variation of office occupancy over time. This model considers China's population density and office habits, as shown in Figure 8.

### Component and structural fragility functions

In the process of structural resilience analysis, it is essential to determine the fragility functions of both components and structures. The fragility functions for components can be defined by specifying the repair methods and cost information corresponding to different damage states. This allows for assessing the direct economic losses needed for repairing earthquake-damaged buildings and the indirect economic losses resulting from using different retrofitting methods. Meanwhile, the majority of casualties result from partial or complete building collapse. To estimate potential casualties, defining the probability of structural collapse as a function of ground motion intensity is essential. These probabilities are typically represented through collapse fragility functions.

*Component fragility functions*

(1) Beam-column components

The PACT software provides an extensive database of fragility functions for structural components, including structural components, non-structural components, and internal financial units. However, the fragility functions of the structural components are established from statistical test information on ductile components. Due to the significant difference in the failure characteristics and the deformation capacity corresponding to the performance points of ductile and non-ductile components, using the fragility functions of ductile structural components for low-ductility RC frame structures resilience assessment would underestimate the deformation damage and structural losses caused by earthquakes. According to existing research [22], insufficient stirrup configuration is the primary cause of low ductility for RC components. Current standards [19,20] specify that the volumetric stirrup ratio in confined regions of column components must exceed 0.4% to ensure the sufficient ductility of RC components under earthquake actions. Therefore, components with a volumetric stirrup ratio of less than 0.4% are defined as low-ductility components. A database containing 46 low-ductility components and 113 FRP-reinforced low-ductility components has been established to predict structural losses more accurately. Detailed information can be seen in reference [31].

According to reference [32], the damage states of RC columns are categorized into six levels, including slight damage, minor damage, moderate damage, slight severe damage, severe damage, and collapse. These damage states are labeled as DS1 to DS6, respectively. The damage phenomena and repair methods corresponding to each state are detailed in reference [33,34]. The performance points are obtained from the column's backbone curve, as shown in Figure 9. Points B and C represent the nominal yield point ($M_y = 0.8M_p$) and peak

**Table 1. Carbon emissions result for case structures**

| Material | Type | Concrete | Steel | CFRP fabric |
|---|---|---|---|---|
| | Unit | $m^3$ | t | $m^2$ |
| | Consumption | 399.24 | 35.43 | 301.44 |
| Transportation distance / km | | 40 | 500 | 500 |
| Carbon emission factor ($tCO_{2e}$/unit) | | 0.316 | 2.34 | 0.14 |
| Production carbon emissions ($tCO_{2e}$) | | 169.69 | 1,852.39 | 42.2 |
| Transportation carbon emissions ($tCO_{2e}$) | | 10.31 | 79.16 | 30.14 |
| Total carbon emissions ($tCO_{2e}$) | | 2,111.56 for case-1<br>2,183.91 for case-2 | | |

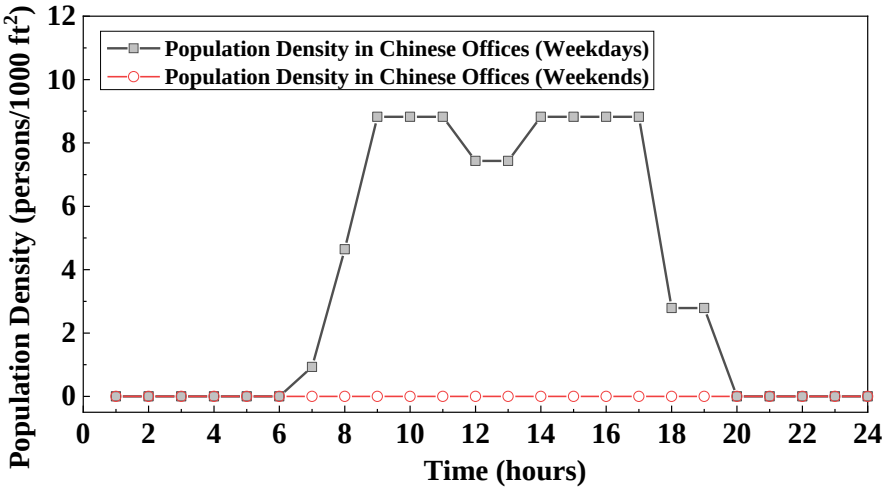


**Figure 8.** Population density model for office building in China.

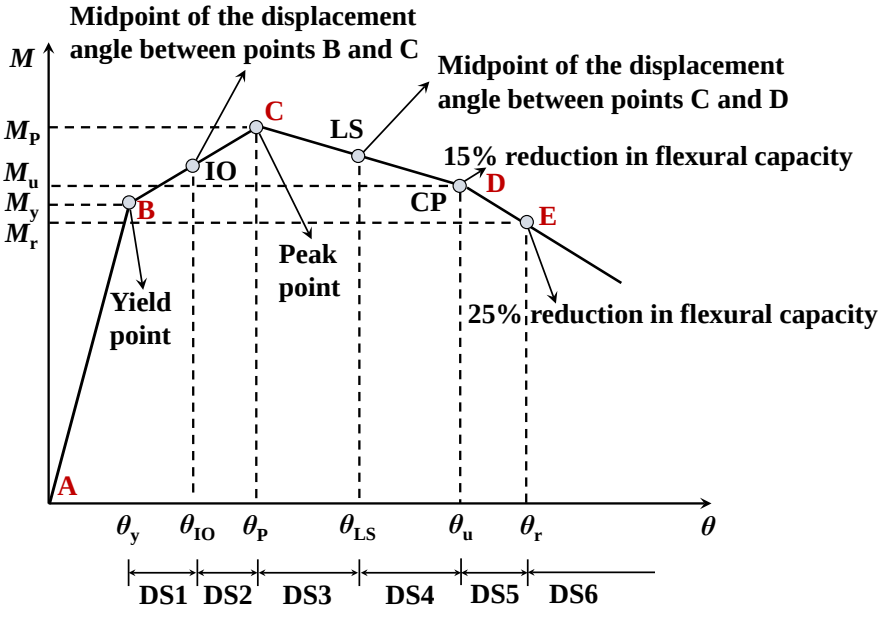


**Figure 9.** Definition of performance points.

point of the backbone curve, respectively. Points D and E correspond to a 15% and 25% reduction from the peak moment, respectively. IO (Immediate Occupancy) is defined as the midpoint of the displacement angle

between points B and C, LS (Life Safety) is the midpoint between points C and D, and the state beyond point E is defined as collapse.

Since there is significant variability in the fragility function of the components at different ACRs, the fragility functions of the components are established by considering the factor of ACR. With an ACR of 0.3 as the boundary, specimens with ACR less than or equal to 0.3 are classified as low-ACR specimens, while those with ACR greater than 0.3 are classified as high-ACR specimens. Based on the ACR and FRP retrofitting characteristics, all specimens in the database are divided into four groups, including low-ACR low-ductility (LAND) group, high-ACR low-ductility (HAND) group, low-ACR FRP-reinforced low-ductility (LAFND) group, and high-ACR FRP-reinforced low-ductility (HAFND) group.

The characteristic points of the backbone curves for each group of specimens are extracted in Figure 9. After removing outliers using the Peirce criterion, the parameters of the fragility functions are calculated using

$$\theta_i = e^{\left(\frac{1}{M}\sum_{j=1}^{M}\ln(d_j)\right)} \tag{18}$$

$$\beta_i = \sqrt{\beta_{r,i}^2 + \beta_{u,i}^2} \tag{19}$$

where $\theta_i$ and $\beta_i$ are the median value and logarithmic standard deviation of the fragility function.

The parameters of the fragility functions for low-ductility RC columns and FRP-reinforced low-ductility RC columns with different ACRs are shown in Table 2.

Table 2 shows that the median value $\theta$ of the fragility functions for low ACR columns is always higher than that for high ACR columns. This indicates that low ACR columns have significantly greater deformation capacity than high ACR columns. Furthermore, comparing the low-ductility columns before and after FRP retrofitting under the same damage states, it is evident that FRP reinforced substantially enhances the deformation capacity of the components. Additionally, it should be noted that for components reinforced with FRP, it is only worthwhile to be repaired if it is in a state of minor damage. The repair cost will exceed the replacement cost if the damage is severe. This study does not consider repair in such cases and will directly proceed with component replacement. Therefore, the low-ductility columns reinforced with FRP are irreparable in damage states DS4, DS5, and DS6. Consequently, the repair costs, repair time, and carbon emissions of these states are accounted for as complete replacements.

(2) Component categories and fragility function numbers

Referring to the fragility categories of components defined in PACT, the number of components in the four-story structure is calculated based on different directions and floors. The results are presented in Table 3.

*Collapse fragility curve and casualties*

The seismic fragility analysis of the structure before and after FRP retrofitting is conducted using 22 sets of far-field ground motions recommended by FEMA P695[35]. For each set of ground motions, a random direction is selected as the seismic input. The selected ground motion response spectra are shown in Figure 10. Subsequently, incremental dynamic analysis (IDA) is performed to assess the collapse fragility of the structure. According to the method defined in FEMA 350[36], a structure is considered to have collapsed when the tangent stiffness of the IDA curve drops to 20% of the initial elastic stiffness or when the maximum inter-story drift

**Table 2. Fragility functions for low-ductility RC columns before and after FRP retrofitting**

| Component type | Damage state | Group | $\theta$ (%) | $\beta$ | Group | $\theta$ (%) | $\beta$ |
|---|---|---|---|---|---|---|---|
| Low-ductility RC columns B1041.000a(b) | DS1 | LAND | 0.574 | 0.533 | HAND | 0.413 | 0.778 |
| | DS2 | | 0.971 | 0.549 | | 0.732 | 0.628 |
| | DS3 | | 1.353 | 0.574 | | 1.039 | 0.597 |
| | DS4 | | 1.634 | 0.594 | | 1.31 | 0.486 |
| | DS5 | | 1.923 | 0.619 | | 1.636 | 0.45 |
| | DS6 | | 1.937 | 0.58 | | 1.596 | 0.381 |
| FRP-reinforced low-ductility RC columns B1041.010a(b) | DS1 | LAFND | 0.682 | 0.686 | HAFND | 0.622 | 0.838 |
| | DS2 | | 1.431 | 0.78 | | 0.961 | 0.787 |
| | DS3 | | 2.193 | 0.825 | | 1.445 | 0.811 |
| | DS4 | | 2.897 | 0.792 | | 2.005 | 0.758 |
| | DS5 | | 3.954 | 0.7 | | 2.523 | 0.744 |
| | DS6 | | 4.498 | 0.659 | | 3.304 | 0.815 |

**Table 3. Component categories and fragility function numbers**

| Direction | Component type | Fragility number | Unit | Numbers of floor | | |
|---|---|---|---|---|---|---|
| | | | | Floor 1 | Floor 2-4 | Roof |
| X direction | **Structural components** | | | | | |
| | Beam-column components (select one) | B1041.000 (low-ductility) | pcs | 24 | 24 | — |
| | | B1041.010 (FRP-reinforced) | pcs | 24 | 24 | — |
| | **Non-structural components** | | | | | |
| | Non-structural exterior walls | B1052.001 | 9.29 $m^2$ | 15.5 | 13.56 | — |
| | Non-structural interior walls | C1011.001a | 120.77 $m^2$ | 2.38 | 2.09 | — |
| | Exterior wall finishes | C3011.002a | 83.61 $m^2$ | 1.72 | 1.51 | — |
| | Interior wall finishes | C3011.001a | 83.61 $m^2$ | 6.89 | 6.03 | — |
| Y direction | **Structural components** | | | | | |
| | Beam-column components (select one) | B1041.000 (low-ductility) | pcs | 24 | 24 | — |
| | | B1041.010 (FRP-reinforced) | pcs | 24 | 24 | — |
| | **Non-structural components** | | | | | |
| | Non-structural exterior walls | B1052.001 | 9.29 $m^2$ | 31 | 27.13 | — |
| | Non-structural interior walls | C1011.001a | 120.77 $m^2$ | 2.38 | 2.09 | — |
| | Exterior wall finishes | C3011.002a | 83.61 $m^2$ | 3.44 | 3.01 | — |
| | Interior wall finishes | C3011.001a | 83.61 $m^2$ | 6.89 | 6.03 | — |
| Non-directional | **Other components** | | | | | |
| | Ceiling | C3032.003b | 55.74 $m^2$ | 8.07 | 8.07 | — |
| | HVAC pipes | D3041.011a | 30.48 m | 6.89 | 6.89 | — |
| | Firefighting pipes | D4011.021a | 30.48 m | 6.89 | 6.89 | — |
| | Roof | B3011.013 | 9.29 $m^2$ | — | — | 48.44 |
| | Chiller | D3031.013h | pcs | — | — | 1 |
| | Air handling unit | D3052.013k | pcs | — | — | 1 |

exceeds the limit of 0.1. According to reference[37], the collapse points are fitted to a lognormal distribution using the maximum likelihood estimation method.

The collapse fragility curves for Case-1 (unreinforced) and Case-2 (FRP-reinforced) structures are shown in Figure 11. The median and logarithmic standard deviation of the fragility function for Case-1 are 0.744 and 0.602, respectively, while for Case-2, they are 0.828 and 0.541, respectively. This indicates that FRP retrofitting reduces the probability of structural collapse. Assuming that the building collapses with the sidesway failure, the fatality rate and injury rate for the collapse of RC frame structures are assumed to be 15% and 85%, respectively according to reference[38].

### Residual drift

Residual drift fragility represents the probability that a structure can be repaired when residual inter-story drift is present after an earthquake. If the building cannot be repaired, the repair costs, repair time, carbon emissions, and energy consumption are assumed to equal those of complete replacement. According to the residual drift fragility function provided in FEMA P-58[13], the median value is 1%, and the standard deviation

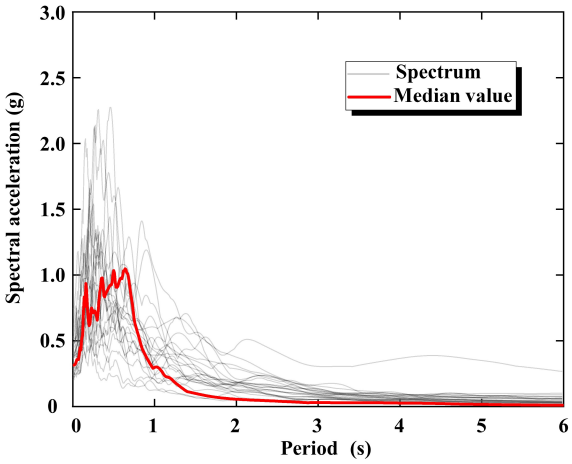


**Figure 10.** Response spectrum and median value.

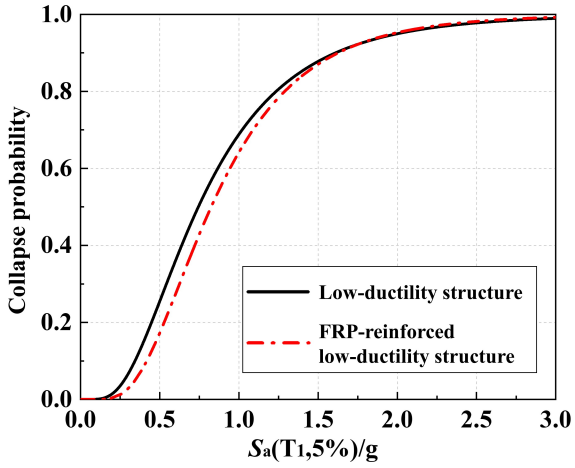


**Figure 11.** Collapse fragility curves.

is 0.3. The calculation method for structural residual drift is given by:

$$\begin{aligned} \Delta_r &= 0 && \Delta \le \Delta_y \\ \Delta_r &= 0.3(\Delta - \Delta_y) && \Delta_y < \Delta < 4\Delta_y \\ \Delta_r &= \Delta - 3\Delta_y && \Delta \ge 4\Delta_y \end{aligned} \tag{20}$$

where $\Delta$ is the inter-story drift obtained through numerical simulation; $\Delta_y$ is the inter-story drift calculated at the yield point of the structure, which corresponds to the maximum inter-story drift at the yield point on the pushover curve; $\Delta_r$ is the overall residual drift of the structure.

### Seismic hazard curve

Using the seismic hazard analysis function proposed by Cornell [39], the hazard function $H(x)$ can be approximated by an exponential form, as

$$H(x) \approx k_0 x^{-k} \tag{21}$$

where $H(x)$ is the annual exceedance probability of a certain intensity earthquake occurring at the design site; $k_0$ and $k$ are parameters related to the design site and other factors.

According to reference[40] and Chinese seismic code[19], $k_0$ and $k$ can be calculated as follows:

$$k = \frac{\ln(\lambda_D/\lambda_M)}{\ln(I_M/I_D)} \tag{22}$$

$$\ln(k_0) = \ln\left[\lambda_D(I_{M_D})^k\right] = \frac{\ln(I_{M_D})\cdot\ln(\lambda_M) - \ln(I_M)\cdot\ln(\lambda_D)}{\ln\left(I_{M_D}/I_M\right)} \tag{23}$$

where $\lambda_D$ and $\lambda_M$ are the annual exceedance probabilities for the design-based earthquake (DBE) and the MCE, respectively. These probabilities can be calculated based on their return periods, $\lambda_D = 1/475 = 0.0021$ and $\lambda_M = 1/2475 = 0.0004$; $IM_D$ and $IM_M$ are the seismic intensity parameters corresponding to the DBE and MCE in the seismic code, with spectral acceleration $S_a$ being used in this study. Substituting into Equations (22) and (23) yields $k = 1.84$ and $k_0 = 1.35 \times 10^{-5}$.

According to reference[13], eight seismic intensities are selected for structural resilience assessment. The 22 ground motions above are amplitude-modulated to these eight seismic intensities, followed by the structural resilience assessment based on the dynamic time-history analysis data. The selected seismic intensities and the calculated annual exceedance rate are shown in Table 4. The seismic hazard curve for the structure's site is presented in Figure 12.

## RESULT ANALYSIS

### Retrofitting impact factor (RIF)

This study introduces the retrofitting impact factor (RIF) as an indicator to quantify the extent to which FRP retrofitting affects the seismic resilience of low-ductility structures, which is calculated by:

$$\delta = \frac{D_{ND} - D_{(ND-C)}}{D_{ND}} \times 100\% \tag{24}$$

where $D_{ND}$ represents the resilience indicators (replacement costs, replacement time, casualties, *etc*.) for the low-ductility structure; $D_{ND-C}$ indicates the resilience indicators (replacement costs, replacement time, casualties, *etc*.) for the low-ductility structure after FRP retrofitting.

### Repair cost

Based on 1000 Monte Carlo simulations, the average repair costs for the case structure under eight different seismic intensities are obtained, as shown in Table 5. The table indicates that FRP retrofitting can reduce the repair costs by up to 9.26% at Intensity 1. However, as the seismic intensity increases, the effectiveness of FRP retrofitting in reducing repair costs gradually decreases. This is because, at very high seismic intensities, although the collapse probability of Case-2 is lower than that of Case-1, a significant number of structural components in Case-2 reach or exceed DS4. As a result, most simulation results indicate a complete replacement of the structure. Additionally, the repair cost calculations for Case-2 include the costs of FRP retrofitting. This results in a negative $\delta$ in some cases, indicating that FRP retrofitting is ineffective.

**Table 4. Seismic intensities and the corresponding annual rate of exceedance**

| Number | Intensity 1 | Intensity 2 | Intensity 3 | Intensity 4 | Intensity 5 | Intensity 6 | Intensity 7 | Intensity 8 |
|---|---|---|---|---|---|---|---|---|
| $S_a$ | 0.052 | 0.088 | 0.124 | 0.16 | 0.196 | 0.231 | 0.267 | 0.303 |
| Annual exceedance rate ($10^{-4}$) | 44 | 13.3 | 6.57 | 3.97 | 2.73 | 2 | 1.54 | 1.18 |

**Table 5. Repair cost and RIF**

| Repair cost (×10⁴ dollar) | Intensity 1 | Intensity 2 | Intensity 3 | Intensity 4 | Intensity 5 | Intensity 6 | Intensity 7 | Intensity 8 |
|---|---|---|---|---|---|---|---|---|
| Case-1 | 17.78 | 35.44 | 44.75 | 50.98 | 53.65 | 54.18 | 54.72 | 55.32 |
| Case-2 | 16.14 | 33.22 | 44.28 | 51.08 | 53.41 | 54.42 | 55.13 | 55.77 |
| *RIF* $\delta$ (%) | 9.26 | 6.26 | 1.05 | -0.2 | 0.44 | -0.45 | -0.75 | -0.8 |

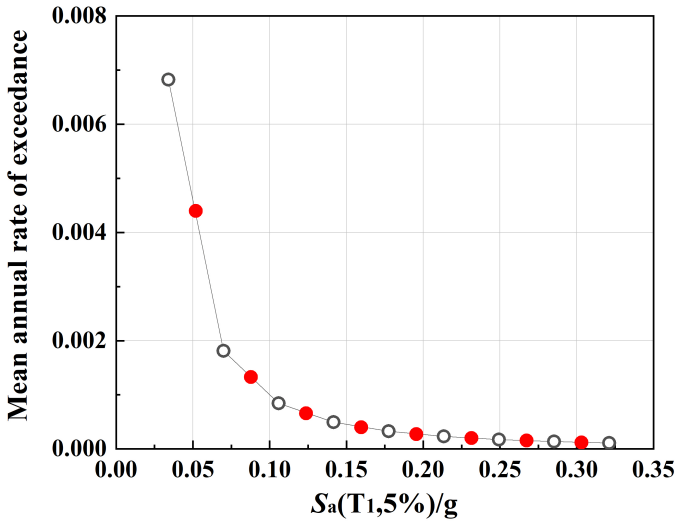


**Figure 12.** Seismic hazard curve.

Based on the classification of component fragility, the structure's repair costs are divided into three categories, including exterior components, interior components, and service systems. The proportion of total repair costs for these categories under eight seismic intensities is shown in Figure 13. It is clear that the proportion of losses attributed to interior components and service systems grows with seismic intensity for both Case-1 and Case-2. This is due to the increased damage to non-structural components such as partition walls, pipes, and ceilings, as well as service systems, resulting in a higher proportion of their repair costs in the total repair costs. This implies that FRP seismic retrofitting does not significantly decrease the damage levels of interior components and service systems.

By combining the site's seismic hazard, the time-based method is further used to assess the seismic resilience of the structure. The annual repair cost probability distribution is shown in Figure 14. It can be observed that the average annual repair costs before and after FRP retrofitting are $1,520.81 and $1,439.84, respectively. This indicates that FRP retrofitting can reduce the average annual repair costs of low-ductility structures by 5.32%.

### Repair time

Based on Monte Carlo simulations and considering the total replacement time of the structure, the average repair times for the case structure under eight different seismic intensities are obtained, as shown in Table 6.

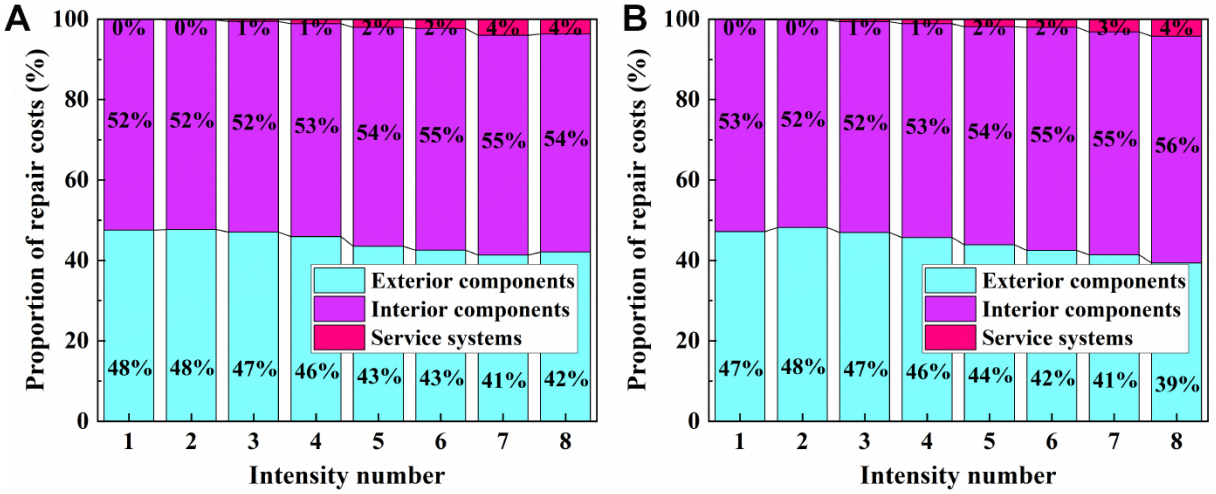


**Figure 13.** Repair cost for three categories. (A) Case-1; (B) Case-2.

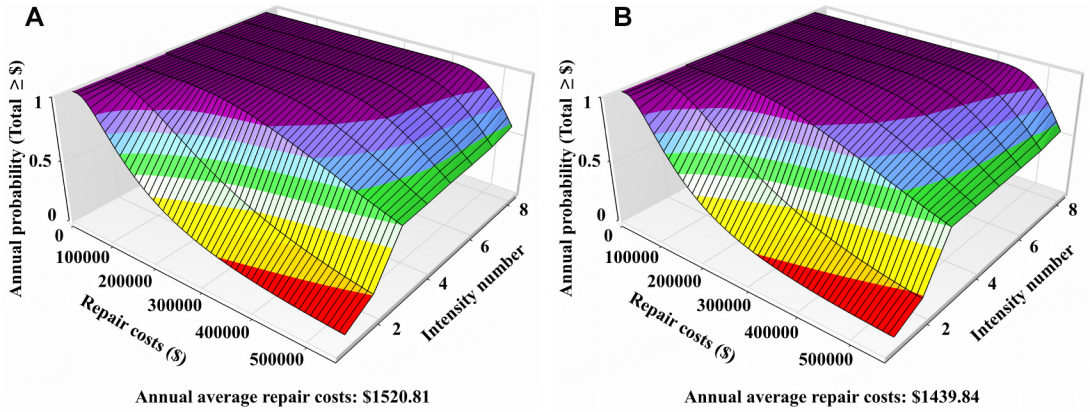


**Figure 14.** Annual repair cost probability distribution. (A) Case-1; (B) Case-2.

**Table 6. Repair time and RIF**

| Repair time (days) | Intensity 1 | Intensity 2 | Intensity 3 | Intensity 4 | Intensity 5 | Intensity 6 | Intensity 7 | Intensity 8 |
|---|---|---|---|---|---|---|---|---|
| Case-1 | 60.61 | 117.08 | 155.49 | 186.02 | 209.78 | 219.16 | 231.79 | 234.96 |
| Case-2 | 55.8 | 107.63 | 148.98 | 180.75 | 201.24 | 211.77 | 226.25 | 234.94 |
| *RIF δ (%)* | 7.94 | 8.07 | 4.19 | 2.84 | 4.07 | 3.37 | 2.39 | 0.01 |

From Table 6, it is evident that FRP retrofitting consistently reduces the repair time across all intensity levels. Notably, for the Case-2 structure at intensity level 2, the repair time is reduced by up to 8.07%. However, at very high seismic intensities, many structural components in Case-2 reach or exceed DS4, rendering them irreparable and causing the repair time to approach the total replacement time. In such cases, FRP retrofitting becomes ineffective in reducing repair time.

The distribution of repair time across different floors of the case structures under eight seismic intensities is shown in Figure 15. For both case structures, the repair time for the first floor is the highest, accounting for approximately 30%, while the repair times for the other three floors are relatively similar.

The time-based evaluation method is further used to assess the seismic resilience of the structure, resulting in the annual repair time probability distribution shown in Figure 16. The calculations reveal that the average

**Table 7. Number of fatalities and RIF**

| Number of fatalities | Intensity 1 | Intensity 2 | Intensity 3 | Intensity 4 | Intensity 5 | Intensity 6 | Intensity 7 | Intensity 8 |
|---|---|---|---|---|---|---|---|---|
| Case-1 | 0 | 0.0245 | 0.0099 | 0.0114 | 0.1407 | 0.2114 | 0.4927 | 0.6937 |
| Case-2 | 0 | 0 | 0 | 0 | 0 | 0.101 | 0.2405 | 0.3242 |
| *RIF* $\delta$(%) | - | 100 | 100 | 100 | 100 | 52.2 | 51.19 | 53.26 |

**Table 8. Number of injuries and RIF**

| Number of injuries | Intensity 1 | Intensity 2 | Intensity 3 | Intensity 4 | Intensity 5 | Intensity 6 | Intensity 7 | Intensity 8 |
|---|---|---|---|---|---|---|---|---|
| Case-1 | 0.0016 | 0.1397 | 0.0592 | 0.0876 | 0.8239 | 1.2328 | 2.8967 | 4.0142 |
| Case-2 | 0 | 0.0006 | 0.0039 | 0.0276 | 0.286 | 0.6095 | 1.5244 | 1.9492 |
| *RIF* $\delta$(%) | 100 | 99.6 | 93.41 | 68.44 | 65.28 | 50.56 | 47.37 | 51.44 |

**Table 9. Carbon emissions and RIF**

| Carbon emissions (×104 kg) | Intensity 1 | Intensity 2 | Intensity 3 | Intensity 4 | Intensity 5 | Intensity 6 | Intensity 7 | Intensity 8 |
|---|---|---|---|---|---|---|---|---|
| Case-1 | 23.83 | 56.86 | 85.96 | 108.53 | 131.69 | 143.53 | 160.5 | 164.02 |
| Case-2 | 21.34 | 53.69 | 84.09 | 109.9 | 128.8 | 141.99 | 161.1 | 171.06 |
| *RIF* $\delta$(%) | 10.43 | 5.57 | 2.17 | -1.26 | 2.2 | 1.07 | -0.38 | -4.29 |

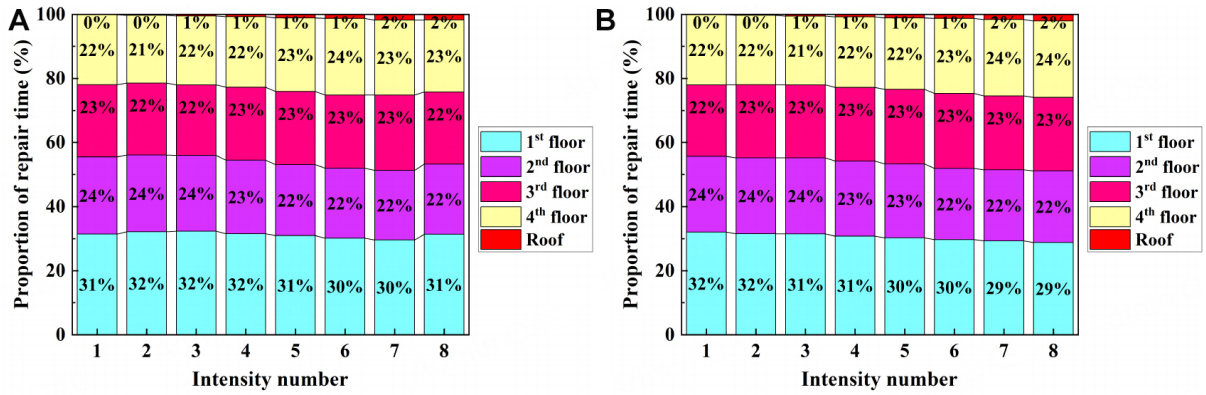


**Figure 15.** Repair time for different floors. (A) Case-1; (B) Case-2.

annual repair time for Case-1 is 0.2393 days, whereas for Case-2, it is 0.2228 days. This indicates that FRP retrofitting reduces the average annual repair time of low-ductility structures by 6.90%.

## Casualties

The average numbers of fatalities and injuries under eight different seismic intensities are shown in Tables 7 and 8. Tables 7 and 8 show that as the intensity level rises, the number of fatalities and injuries in the structure gradually increases. Compared to the low-ductility structure, the number of fatalities and injuries in the FRP-reinforced structure is significantly reduced. Comparing the two case structures at different intensities, the Case-1 structure shows potential fatalities and injuries at intensity levels 1 and 2. In contrast, the Case-2 structure exhibits fatalities and injuries only at intensity levels 2 and 6, respectively. This indicates that FRP retrofitting can significantly reduce the casualty rate for occupants. Furthermore, it can be observed that as the intensity level increases, the value of $\delta$ gradually decreases. At intensity level 8, $\delta$ decreases to approximately 50%. This suggests that the benefits of FRP retrofitting in terms of casualty reduction diminish at higher intensity levels. However, it is noteworthy that as the intensity level grows, the reduction in casualties for Case-2 compared to Case-1 progressively increases.

Figures 17 and 18 present the probability distributions of the annual average fatalities and injuries for the example structure. From these figures, it can be seen that the estimated annual average number of fatalities for

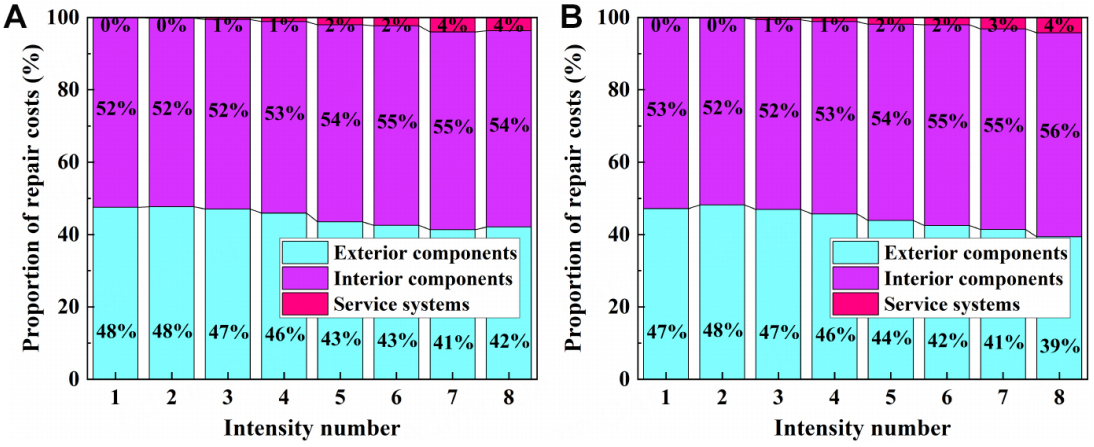


**Figure 16.** Annual repair time probability distribution. (A) Case-1; (B) Case-2.

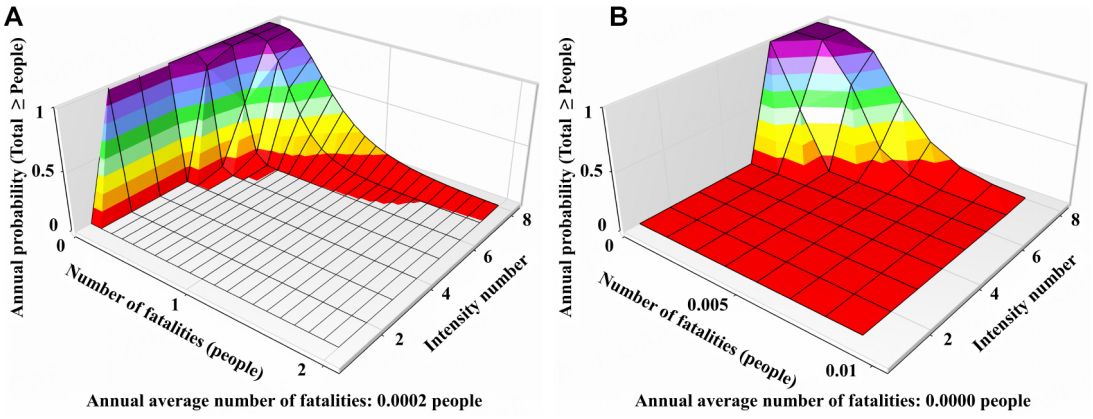


**Figure 17.** Annual number of fatalities probability distribution. (A) Case-1; (B) Case-2.

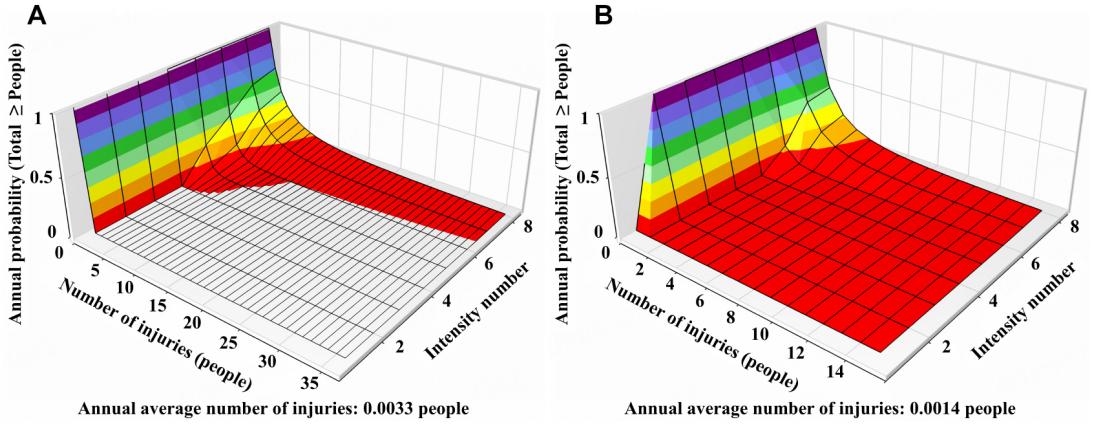


**Figure 18.** Annual number of injuries probability distribution. (A) Case-1; (B) Case-2.

the Case-1 structure is 0.0002, while after FRP retrofitting, the annual average number of fatalities decreases to nearly zero. Additionally, comparing the annual average number of injuries for the two structures, it is evident that FRP retrofitting significantly reduces the probability of injuries, with the annual average number of injuries

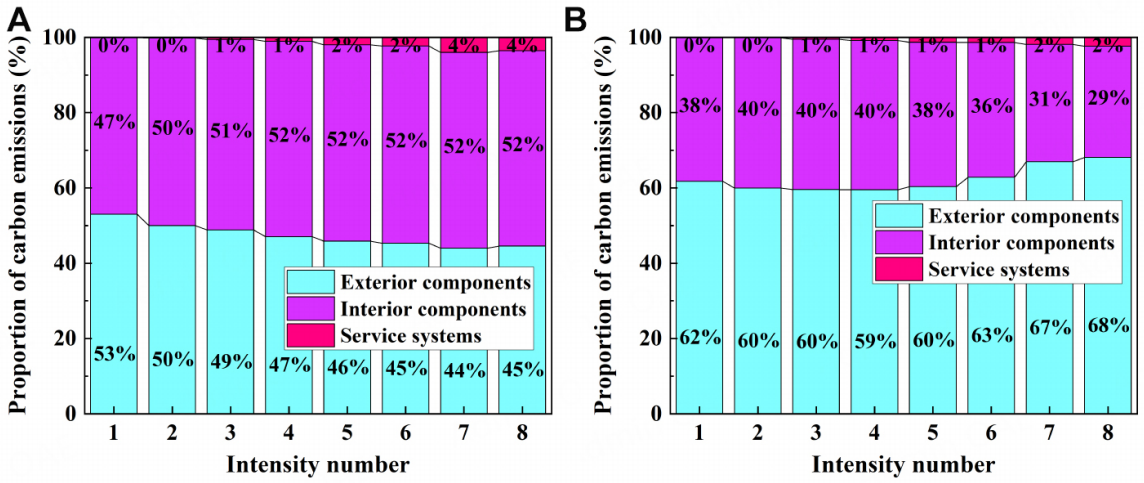


**Figure 19.** Carbon emissions for three categories. (A) Case-1; (B) Case-2.

decreasing from 0.0033 in the low-ductility structure to 0.0014 in the FRP-reinforced structure. The reduction reaches 57.6%. These results highlight the effectiveness of FRP retrofitting in enhancing the seismic resilience of structures and reducing casualties, particularly in terms of significantly lowering the annual average number of injuries and fatalities.

### Carbon emissions

The average carbon emissions for Case-1 and Case-2 under eight different seismic intensities are shown in Table 9. The table shows that Case-2 can reduce structural carbon emissions by 10.43% at intensity level 1 compared to Case-1. Additionally, at intensity levels 2, 3, 5, and 6, FRP retrofitting also reduces the carbon emissions of the structure. At higher seismic intensities, numerous components in the Case-2 structure experience severe damage, leading to repair costs that surpass the replacement cost for much of the structure. Additionally, since the carbon emissions associated with Case-2 include the FRP retrofitting process, this results in a negative reduction efficiency ($\delta$) at certain intensity levels.

The proportion of carbon emissions from the replacement of exterior components, interior components, and service systems for the two cases is shown in Figure 19. For the Case-1 structure, the proportion of carbon emissions from interior components and service systems increases with seismic intensity, but the growth trend is not significant. Interior components account for approximately 52%, while service systems reach up to 4%. Compared to Case 1, the carbon emissions required to repair exterior components in the Case-2 structure are higher, exceeding 60%. Conversely, the carbon emissions for repairing interior components in Case-2 are significantly lower, ranging from 30% to 40%. This is because the carbon emissions from steel used in repairs are much higher than those from concrete and FRP fabric. Meanwhile, a large number of non-structural components and wall finishes in interior components do not require a significant amount of steel. Therefore, the carbon emissions during structural repairs are primarily due to exterior components.

Considering seismic hazard, the probability distribution of the annual carbon emissions of the structure is shown in Figure 20. The calculations show that the average annual carbon emissions for the Case-1 structure are 3,050.17 kg, while for Case-2, it is 2,831.89 kg. This indicates that FRP retrofitting can reduce the average annual carbon emissions of low-ductility structures by 7.16%.

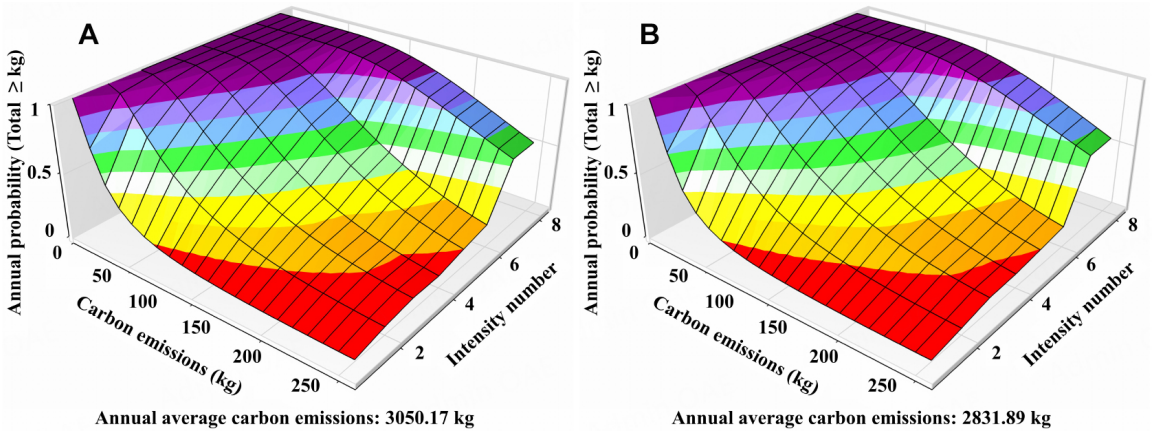


**Figure 20.** Annual number of fatalities probability distribution. (A) Case-1; (B) Case-2.

## CONCLUSION

This study investigates the effect of FRP retrofitting on the resilience of low-ductility structures. The finite element models of low-ductility frame structures and FRP-reinforced low-ductility frame structures are established. Fragility functions for low-ductility structural components before and after FRP retrofitting are developed. Using PACT software, the time-based assessment process is applied to analyze resilience indicators such as repair costs, repair time, casualties, and carbon emissions before and after retrofitting. The main conclusions are as follows:

(1) The study established fragility functions for both low-ductility RC components and FRP-reinforced low-ductility RC components. For low-ductility RC components, the median values of the fragility functions ranged from 0.413 to 1.937, with logarithmic standard deviations between 0.381 and 0.619. In contrast, the median values for FRP-reinforced low-ductility RC components are significantly higher, ranging from 0.622 to 4.498, with logarithmic standard deviations between 0.659 and 0.838;

(2) The benefits of FRP retrofitting are most pronounced at lower seismic intensities. At these levels, FRP retrofitting significantly enhances structural resilience, leading to substantial reductions in repair costs, repair times, and casualty rates. As the seismic intensity increases, the relative effectiveness of FRP retrofitting diminishes;

(3) A detailed quantitative analysis demonstrated that FRP retrofitting significantly reduces the annual exceedance probabilities for repair costs, repair times, casualties, and carbon emissions. The average annual repair costs are reduced by 5.32%, while the average annual repair time decreased by 6.90%. Most notably, FRP retrofitting nearly eliminated the annual average number of fatalities and reduced the annual average number of injuries by 57.6%, highlighting a substantial improvement in safety. Additionally, the average annual carbon emissions are reduced by 7.16%, indicating the environmental benefits of FRP retrofitting alongside enhanced structural resilience.

It should be noted that although a preliminary study on the effect of FRP retrofitting on low-ductility structures has been conducted in this paper, further investigation is required due to the limited research sample. Firstly, only a four-story structure designed for a seismic intensity of seven degrees in a type II site class is considered. Further discussion is needed to determine whether higher seismic fortification levels and different story heights affect the structure. Secondly, the loss model for the structure did not account for the economic development of the region where the structure is located. This may potentially lead to an underestimation of losses in developed

areas. Additionally, the significant impact of the post-earthquake repair path on structural resilience requires further discussion in future studies.

## DECLARATIONS

### Authors' contributions

Methodology, conceptualization, writing - review & editing, funding acquisition: Yu X
Data curation, visualization, writing - original draft: Li Z
Data curation, visualization, writing - review & editing: Jiang Z
Methodology, investigation, writing - original draft, supervision, funding acquisition: Dai K

### Availability of data and materials

Data is available upon request from the authors.

### Financial support and sponsorship

The research in this paper has received financial support from the Natural Science Foundation of China (52278492, 52408564), the China Postdoctoral Science Foundation (project number: 2023M733247), the Natural Science Foundation of Henan Province (project number: 232300421322), and the Central Finance of Guangxi Zhuang Autonomous Region Guides Local Science and Technology Development Funds (project number: 2023ZYZX1003).

### Conflicts of interest

Yu X is a Youth Editorial Board Member of the journal *Disaster Prevention and Resilience*, while the other authors have declared that they have no conflicts of interest.

### Ethical approval and consent to participate

Not applicable.

### Consent for publication

Not applicable.



## REFERENCES

1. Yathon J, Adebar P, Elwood KJ. A detailed inventory of Non-ductile concrete shear wall buildings. *Earthq Spectra* 2017;33:123-45. DOI
2. Jeon JS, Lowes LN, DesRoches R, Brilakis I. Fragility curves for non-ductile reinforced concrete frames that exhibit different component response mechanisms. *Eng Struct* 2015;85:127-43. DOI
3. Wang DY. Experimental and analytical investigation of seismic performance of nonductile RC frames retrofitted with FRP; 2012. (in Chinese). Available from: https://kns.cnki.net/kcms2/article/abstract?v=iAN2XHIMbKszPTwpuXPabTROH0bwAqPhLwAZ4eonNE2AT9s-xGoX1FWZGXrjGshsqIqh1AUqAIXWnXz26-qy3Bv_bNUywrUZxAglDFZsOc-qaQv_T5m73YHayw846giR5z1Uqs7APByXWdgmo6-hms6LVhr_t7zDjvMoDi7HGTs=&uniplatform=NZKPT [Last accessed on 22 Nov 2024].
4. Yuksel E, Ozkaynak H, Buyukozturk O, et al. Performance of alternative CFRP retrofitting schemes used in infilled RC frames. *Constr Build Mater* 2009;24:596-609. DOI
5. Ozkaynak H, Yuksel E, Buyukozturk O, Yalcin C, Dindar AA. Quasi-static and pseudo-dynamic testing of infilled RC frames retrofitted with CFRP material. *Compos B Eng* 2010;42:238-63. DOI
6. Kakaletsis D. Comparison of CFRP and alternative seismic retrofitting techniques for bare and infilled RC frames. *J Compos Constr* 2011;15:565-77. DOI
7. Zhu JT, Wang XL, Xu AD, Weng CH. Experimental study on seismic behavior of RC frames strengthened with CFRP sheets. *Compos Struct* 2011;93:1595-603. DOI
8. Wang Y, Chen W, Li D, Xu H, Zhang F, Guo X. Experimental and numerical investigations of the seismic performance of reinforced concrete frames strengthened with CFRP sheets. *Buildings* 2023;13:2195. DOI

9. Ghobarah A, Said A. Seismic rehabilitation of beam-column joints using FRP laminates. *J Earthquake Eng* 2001;5:113-29. DOI
10. Dai KY, Yu XH, Qian K, Wang DY. Deformation capacity of FRP retrofitted reinforced concrete columns with corroded reinforcing bars. *Eng Struct* 2022;254:113834. DOI
11. Abokwiek R, Abdalla JA, Hawileh RA, El Maaddawy T. RC columns strengthened with NSM-CFRP strips and CFRP wraps under axial and uniaxial bending: experimental investigation and capacity models. *J Compos Constr* 2021;25:04021009. DOI
12. Naser MZ, Hawileh RA, Abdalla JA. Fiber-reinforced polymer composites in strengthening reinforced concrete structures: a critical review. *Eng Struct* 2019;198:109542. DOI
13. Agency FEM. Seismic performance assessment of buildings: FEMA P-58-1. Washington DC; 2012. Available from: https://femap58.atcouncil.org/documents/fema-p-58/24-fema-p-58-volume-1-methodology-second-edition/file [Last accessed on 22 Nov 2024].
14. Cimellaro GP, Fumo C, Reinhorn AM, et al. Quantification of disaster resilience of health care facilities: MCEER-09-0009. New York; 2009. Available from: https://nehrpsearch.nist.gov/static/files/NSF/PB2010103200.pdf [Last accessed on 22 Nov 2024].
15. Standard for seismic resilience assessment of buildings: GB/T 38591-2020. Standards Press of China; 2020. (in Chinese). Available from: https://kns.cnki.net/kcms2/article/abstract?v=iAN2XHIMbKuB0NSmRqHBitzZxLCubYv00dtaSLQhdIVApq9wRcZe0ynBbe81mjNz9rvPZKouo1vc0YFIY-RQPNtVM-cEmQghsoZVHwzQsz2YLZHTDZfkuZvdis7Zu3_uRoeFjte_fD3Ngz2VI7RTtLIMwSLnRXsy&uniplatform=NZKPT [Last accessed on 22 Nov 2024].
16. Bruneau M, Chang SE, Eguchi RT, et al. A framework to quantitatively assess and enhance the seismic resilience of communities. *Earthq Spectra* 2003;19:733-52. DOI
17. Cimellaro GP, Reinhorn AM, Bruneau M. Framework for analytical quantification of disaster resilience. *Eng Struct* 2010;32:3639-49. DOI
18. Samadian D, Ghafory-Ashtiany M, Naderpour H, Eghbali M. Seismic resilience evaluation based on vulnerability curves for existing and retrofitted typical RC school buildings. *Soil Dyn Earthq Eng* 2019;127:105844. DOI
19. Code for Seismic Design of Buildings (GB50011-2010). China Architecture & Building Press; 2010. (in Chinese). Available from: https://www.gongbiaoku.com/book/eo120094gy5?query=GB50011-2010 [Last accessed on 22 Nov 2024].
20. Code for Design of Concrete Structures (GB 50010-2010). China Architecture & Building Press; 2010. (in Chinese). Available from: https://www.gongbiaoku.com/book/75z20095doy?query=GB%2050010-2010 [Last accessed on 22 Nov 2024].
21. Scott BD, Park R, Priestley MJN. Stress-strain behavior of concrete confined by overlapping hoops at low and high strain rates. *ACI Struct J* 1982;79:13-27. DOI
22. Wang Z, Wang D, Smith ST, Lu D. CFRP-confined square RC columns. I: Experimental investigation. *J Compos Constr* 2012;16:150-60. DOI
23. Technical standard for fiber reinforced polymer (FRP) in construction. Beijing: China Planning Press; 2020. (in Chinese). Available from: https://www.gongbiaoku.com/book/chq255564fc?query=gb%2050608-2020 [Last accessed on 22 Nov 2024].
24. Lv DG, Dai KY, Yu XH, Li N. Seismic fragility analysis on non-ductile RC frame structures retrofitted with FRP. *Eng Mech* 2017;34:49-53, 70. (in Chinese). DOI
25. China Construction Engineering Network. Available from: http://www.cecn.org.cn/ [Last accessed on 22 Nov 2024].
26. Pricing and quotation for seismic retrofitting of building structures. China Planning Press; 2008. (in Chinese). Available from: https://www.gongbiaoku.com/ebook/nyf1732bnx [Last accessed on 22 Nov 2024].
27. Wen W, Zhang M, Zhai C, Liu W. Resilience loss factor for evaluation and design considering the effects of aftershocks. *Soil Dyn Earthq Eng* 2019;116:43-9. DOI
28. Zhu HB. Frame - shear wall structure seismic performance evaluation based on the full probability theory; 2015. In Chinese. Available from: https://kns.cnki.net/kcms2/article/abstract?v=iAN2XHIMbKs9bqQDQFk5exq9h7mSEeFiDEZTbO54HcUaN1gFd8gXtNpm0n3XW-HqdYTy92GkXYyULnOWzAMOgv7ojJ8UgWHtNjM9c03q8k6s3SU2tuVXOr9pbpxhTViI8qO8TD6chwmxahVTJTbV51Ss5ToWULsMT5zYj244jDw=&uniplatform=NZKPT [Last accessed on 22 Nov 2024].
29. Standard for calculation of building carbon emissions. China Standard Press; 2019. (in Chinese). Available from: https://www.gongbiaoku.com/book/31h17169x9w?query=%E5%BB%BA%E7%AD%91%E7%A2%B3%E6%8E%92%E6%94%BE%E8%AE%A1%E7%AE%97%E6%A0%87%E5%87%86 [Last accessed on 22 Nov 2024].
30. Design standard for energy efficiency of public buildings. China Standard Press; 2015. (in Chinese). Available from: https://www.gongbiaoku.com/book/zwr24736arg?query=%E5%85%AC%E5%85%B1%E5%BB%BA%E7%AD%91%E8%83%BD%E6%95%88%E8%AE%BE%E8%AE%A1%E6%A0%87%E5%87%86 [Last accessed on 22 Nov 2024].
31. Jiang ZC. Damage and resilience assessment of FRP retrofitted low ductility RC frame structures under mainshock-aftershock sequences. Harbin Institute of Technology; 2023. (in Chinese). Available from: https://kns.cnki.net/kcms2/article/abstract?v=iAN2XHIMbKuDtoZveX364Bfi8su4lj15DSD1d6lhqPCdmfD0T8uQ5rTJ0OtmvbGAyLSmd1YbfvFyDwx4rXms5i0xS93n06RgRUKQtG6zEP1mGt_aXCSGeyxXeG158Ysl6TVsALW45qWO7YebwFWT4vQvklj8dT9dN2h5xn0Wb6A=&uniplatform=NZKPT [Last accessed on 22 Nov 2024].
32. Standard for anti-collapse design of building structures. China Planning Press; 2022. (in Chinese). Available from: https://www.gongbiaoku.com/book/iy8248644hn?query=%E5%BB%BA%E7%AD%91%E7%BB%93%E6%9E%84%E6%8A%97%E5%80%92%E5%A1%8C%E8%AE%BE%E8%AE%A1%E6%A0%87%E5%87%86 [Last accessed on 22 Nov 2024].
33. Dai KY. Seismic performance and fragility analysis of corroded reinforced concrete columns and frame structures; 2019. (in Chinese). Available from: https://kns.cnki.net/kcms2/article/abstract?v=iAN2XHIMbKt8zEokLPDvITjxFfNznYDwbLgr183hhbN8ppQFQEcD0xaQRmxMBilo7P3nqjP0BrXnU6pWJS8jbh3ytHQZhpFTpBVrw0NP5N7qwtYKxjXIwXfdLJsY4FFrPZfndiUGnrII6UKu8rwJR-Llpy6hQOmcYf3Szeb0Nd0QdoQMQA==&uniplatform=NZKPT [Last accessed on 22 Nov 2024].
34. Dai KY, Yu XH, Lv DG. Fragility functions for reinforced concrete columns. *J Eng Mech* 2024. (in Chinese). DOI
35. FEMA. Quantification of Building Seismic Performance Factors; 2009. FEMA P695. Available from: https://www.atcouncil.org/files/

ATC-63-1TOC.pdf [Last accessed on 22 Nov 2024].
36. FEMA. Recommended Seismic Design Criteria for New Steel Moment Frame Buildings; 2000. FEMA 350. DOI
37. Dai KY, Yu XH, Jiang ZC, Wang D, Qian K. Hysteretic model for corroded reinforced concrete columns retrofitted with FRP. *Constr Build Mater* 2023;380:131207. DOI
38. Dong Y. Seismic resilience rating and decision-making of uniform collapse risk of RC frame-shear wall structures; 2019. (in Chinese). Available from: https://kns.cnki.net/kcms2/article/abstract?v=iAN2XHIMbKtkfe_StC24lv9qi51uzQfqkjHbFPIvX4LeDbWh9Q6hnM7fvYCCRX671_VjWrXKip_qY0BmRY--EeES0gxh_EvjFXst1vTuMV8nf6zzeI3sycgJbYW3__aQeE2EE8yQmbtCfYG-V0UL3M4Xzo0YSS5BUdcex_viN_I=&uniplatform=NZKPT [Last accessed on 22 Nov 2024].
39. Cornell CA. Engineering seismic risk analysis. *Bull Seismol Soc Am* 1968;58:1583-606. DOI
40. Bradley BA, Dhakal RP, Cubrinovski M, Mander JB, MacRae GA. Improved seismic hazard model with application to probabilistic seismic demand analysis. *Earthq Eng Struct D* 2010;36:2211-25. DOI